Supplement of Solid Earth, 13, 323–346, 2022
https://doi.org/10.5194/se-13-323-2022-supplement

Solid Earth
Open Access

Supplement of

Seismic monitoring of the STIMTEC hydraulic stimulation experiment in anisotropic metamorphic gneiss

Carolin M. Boese et al.

Correspondence to: Carolin M. Boese (carolin.boese@gfz-potsdam.de)

Table S1: Data gaps in the continuous recording.

Start Date	Start Time	End Date	End Time	Comment
03.07.2018	13:38:25	03.07.2018	14:27:20	Power outage
14.07.2018	00:57:25	14.07.2018	01:30:59	Unknown
16.07.2018	07:12:20	16.07.2018	07:13:30	Correlate PC time
16.07.2018	07:47:03	16.07.2018	08:22:45	Test USV
17.07.2018	06:56:10	17.07.2018	07:22:30	Test USV
17.07.2018	07:33:41	18.07.2018	07:12:18	False operation
18.07.2018	07:23:29	18.07.2018	07:37:00	Data Check
19.07.2018	07:17:31	19.07.2018	07:53:38	Data Check
20.07.2018	10:33:07	20.07.2018	10:37:45	Data Check
05.08.2018	19:12:58	07.08.2018	13:28:30	Hard drive full

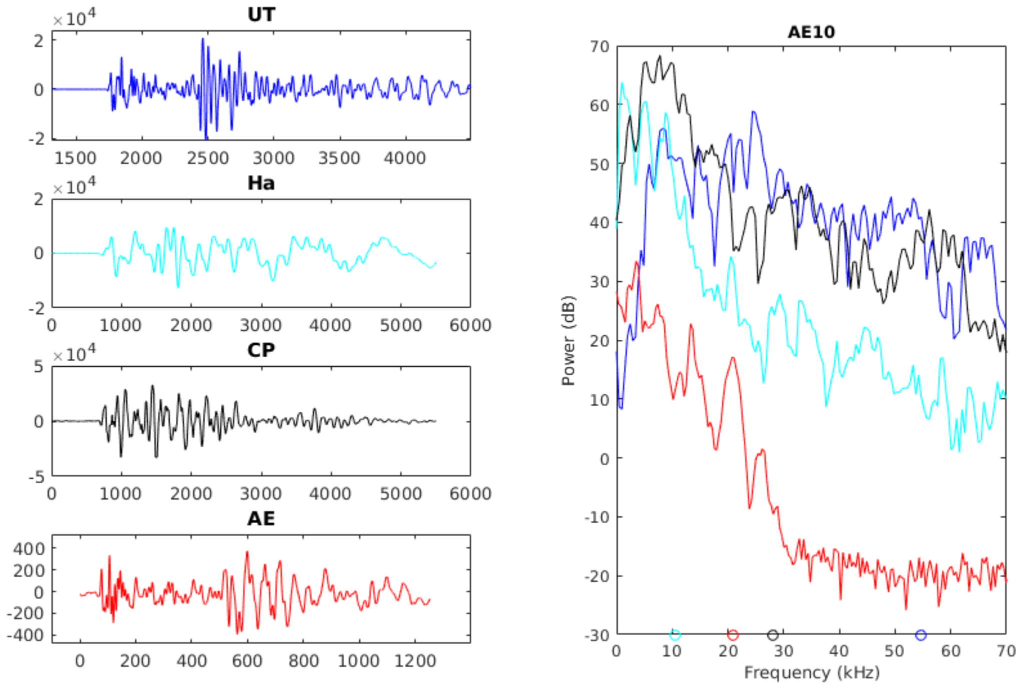

Figure S1: Comparison of the power spectra density of an ultrasonic transmission (UT) signal, a hammer hit (Ha), a centre punch (CP) hit, and an AE event recorded by AE-sensor AE10 (see Figure 4a for location). Note that the AE event occurred slightly offset (at greater depth) compared to the other nearly co-located active source points in the drift way. Also, the sampling rate of the AE event is one fifth of that of the other signals. The power spectral density of the signal is shown on the right with circles indicating the 68% occupied bandwidth of the signal energy.

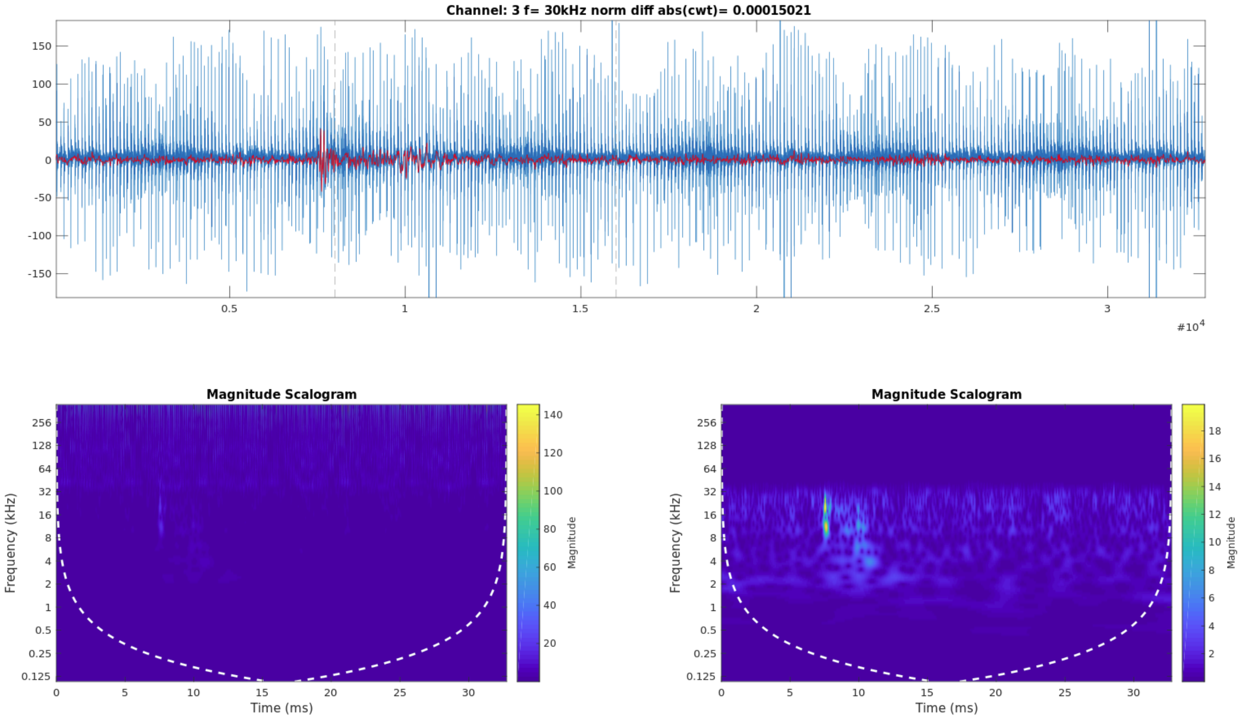

Figure S2: Top: Raw waveform before (blue) and after (red) pump noise suppression at station AE03, which is most of all stations affected by noise. Bottom: Frequency-time plot from continuous wavelet decomposition to determine Morse wavelet coefficients for filtering. We observe that these wavelet coefficients, which dominate the signal in a noise widow before the AE event, are large at high frequencies. By removing these coefficients in the inverse continuous wavelet decomposition, we can effectively suppress the high-amplitude, high-frequency noise.

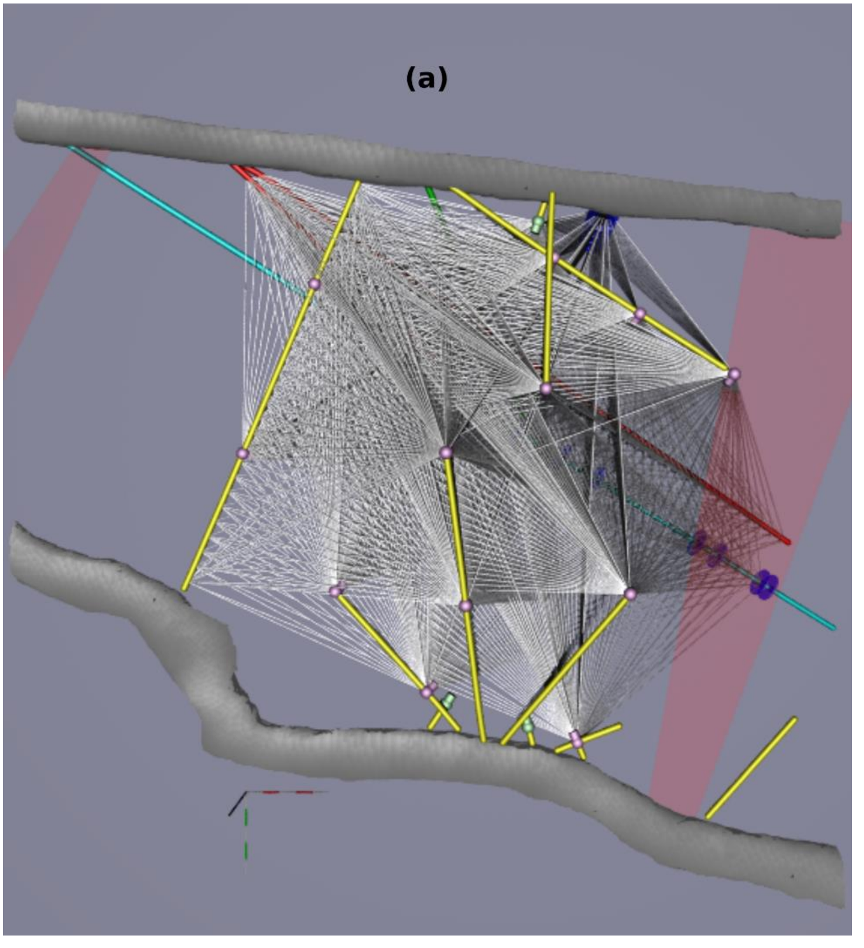
(a)

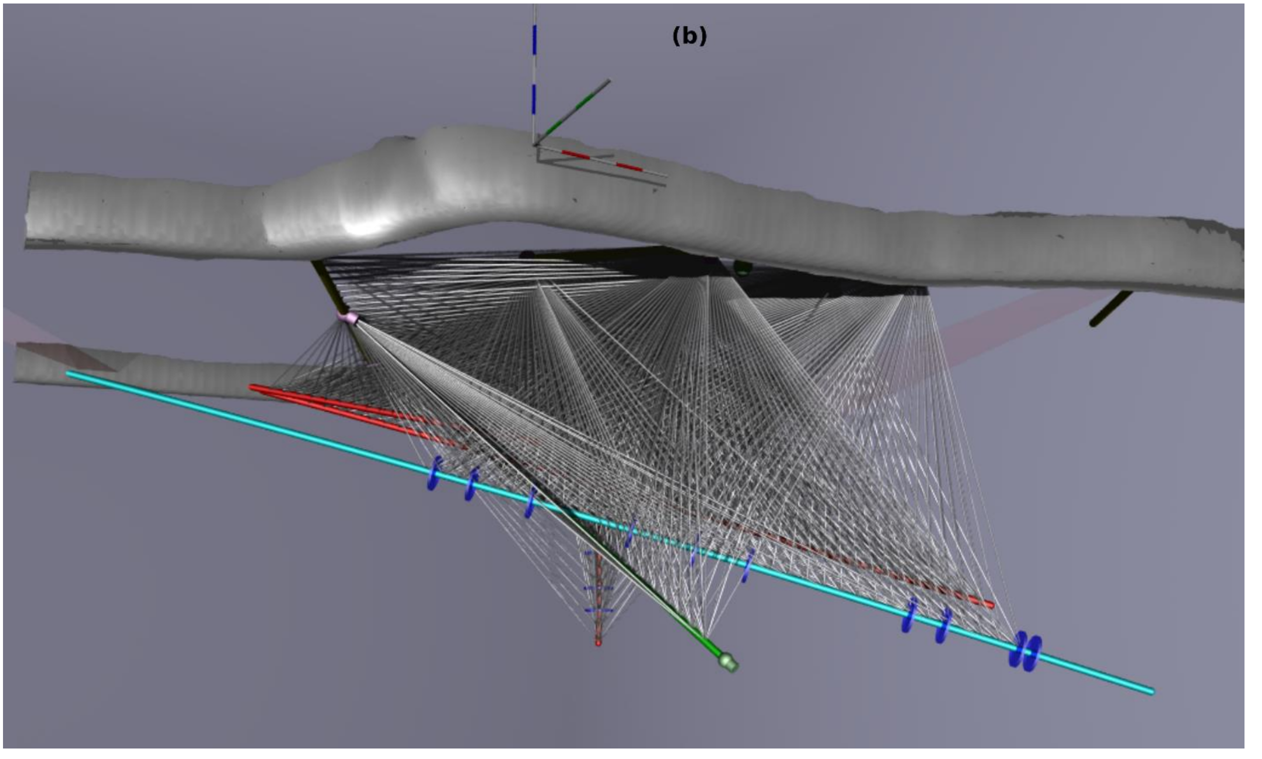
(b)

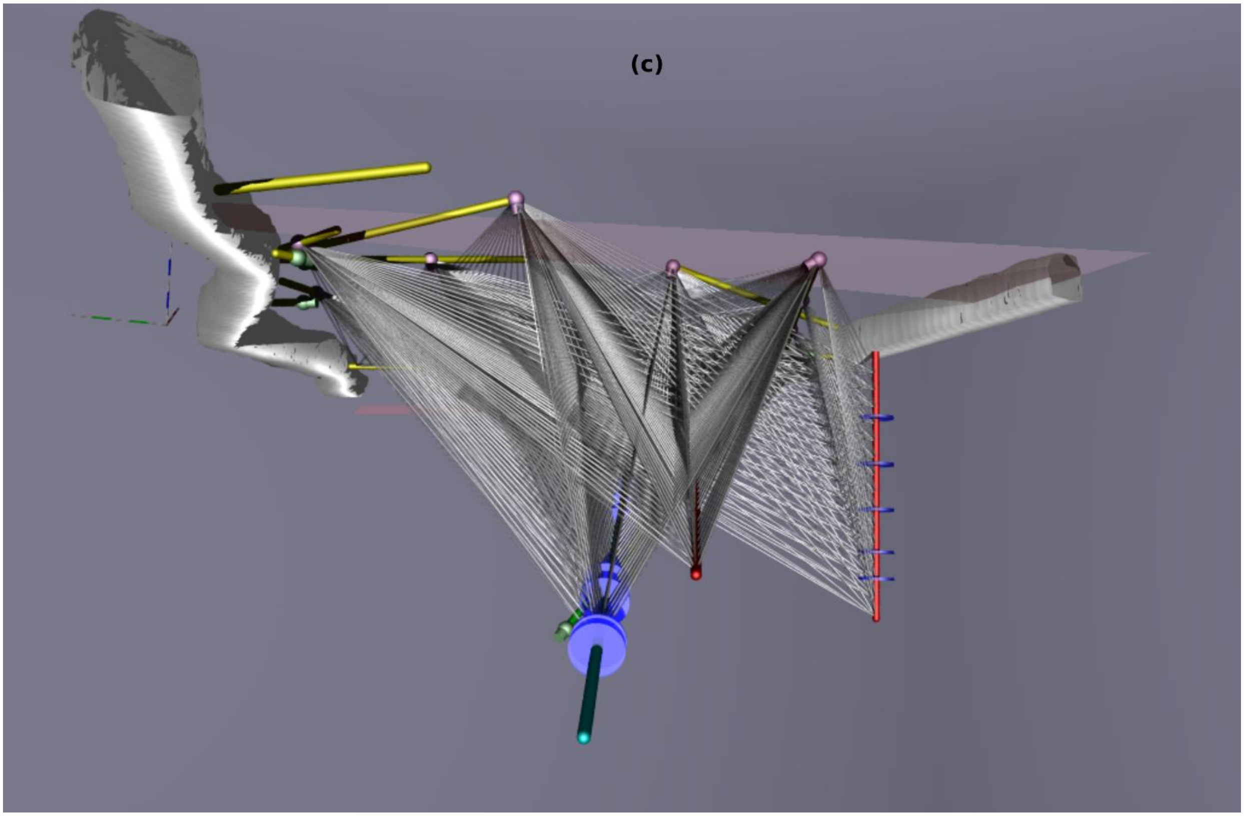

Figure S3: Raypath coverage from known UT measurement points in different boreholes to the AE sensor positions within the STIMTEC volume: View from above (a) and from the side (b,c), looking eastwards (b) and from NE (c) towards the wellhead of the injection borehole in the drift way.

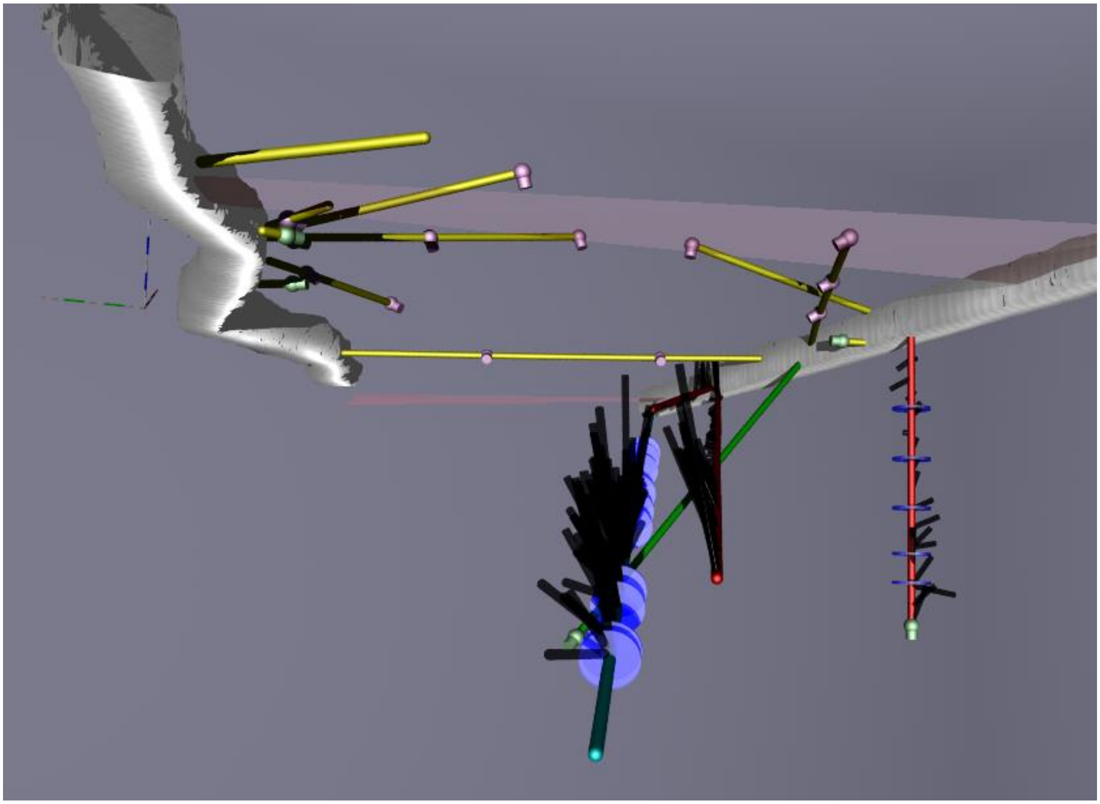

Figure S4: Sideview of the location uncertainty estimates (black lines) along the injection, vertical and horizontal validation boreholes as estimated from locating known UT measurement positions with the derived best transverse isotropic velocity model per seismic sensor. The view is from NE looking towards the wellhead of the injection borehole in drift way.

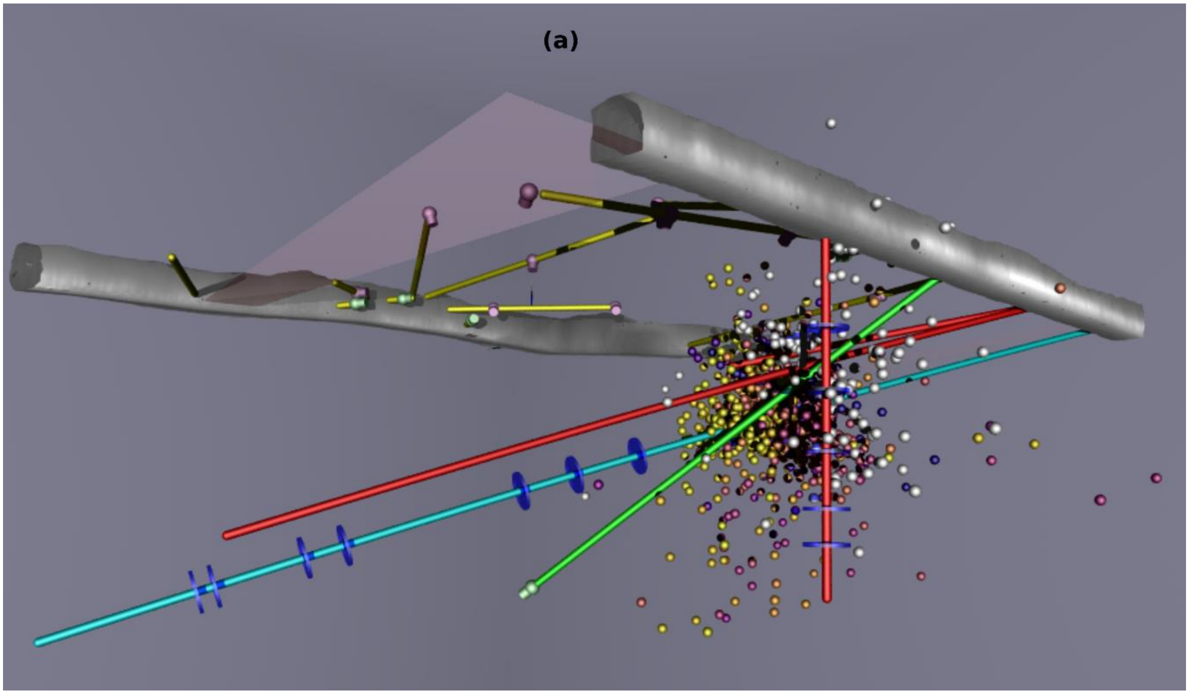
(a)

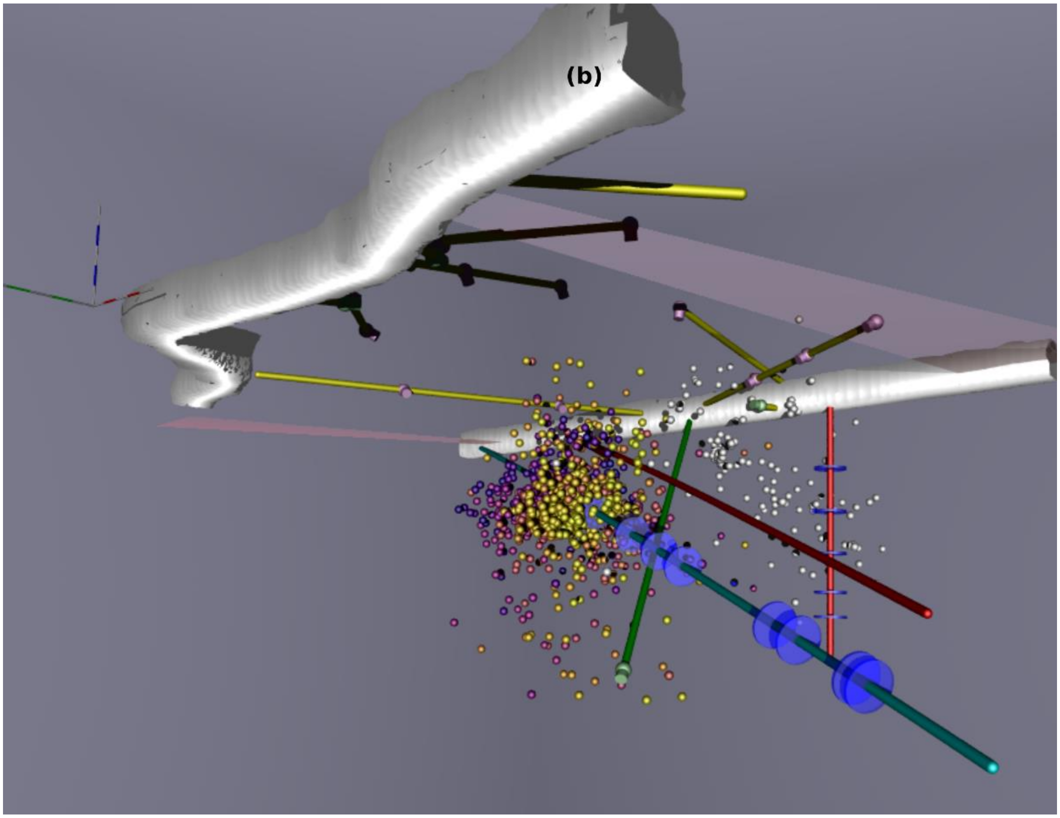

Figure S5: Sideview of the induced AE activity recorded for the injection and vertical validation borehole looking a) towards the Southeast and b) the Southwest. Note that the straight drift way tunnel has an almost North-South orientation.

Table S2: Cross-correlation coefficients obtained for the different stimulation intervals in the injection borehole between pressure and broadband signal and flow rate and broadband signal, respectively. We compared the original broadband and smoothed signals (over 100 and 200 samples, respectively), that where downsampled to 5 samples/second to have the same sampling rate as the pressure and flow rate data. See Figure S6 for a comparison of the resampled and smoothed waveforms.

Interval Hydr. data	Broadband data resampled	smoothed 100x and resampled	smoothed 200x and resampled
HF1 56.5			
P	0.29	0.29	0.27
Q	0.41	0.41	0.41
HF2 51.6			
P	0.42	0.78	0.78
Q	0.37	0.68	0.68

HF3 28.1			
P	0.16	0.27	0.30
Q	0.31	0.49	0.55
HF4 24.6			
P	0.47	0.62	0.62
Q	0.61	0.81	0.81
HF5 33.9			
P	0.30	0.39	0.40
Q	0.54	0.68	0.65
HF6 37.6			
P	0.63	0.81	0.82
Q	0.60	0.77	0.78
HF7 55.7			
P	0.53	0.61	0.61
Q	0.67	0.76	0.74
HF8 49.7			
P	0.32	0.36	0.32
Q	0.62	0.69	0.63
HF9 40.6			
P	0.29	0.36	0.36
Q	0.46	0.56	0.50
HF10 22.4			
P	0.36	0.49	0.48
Q	0.48	0.68	0.69

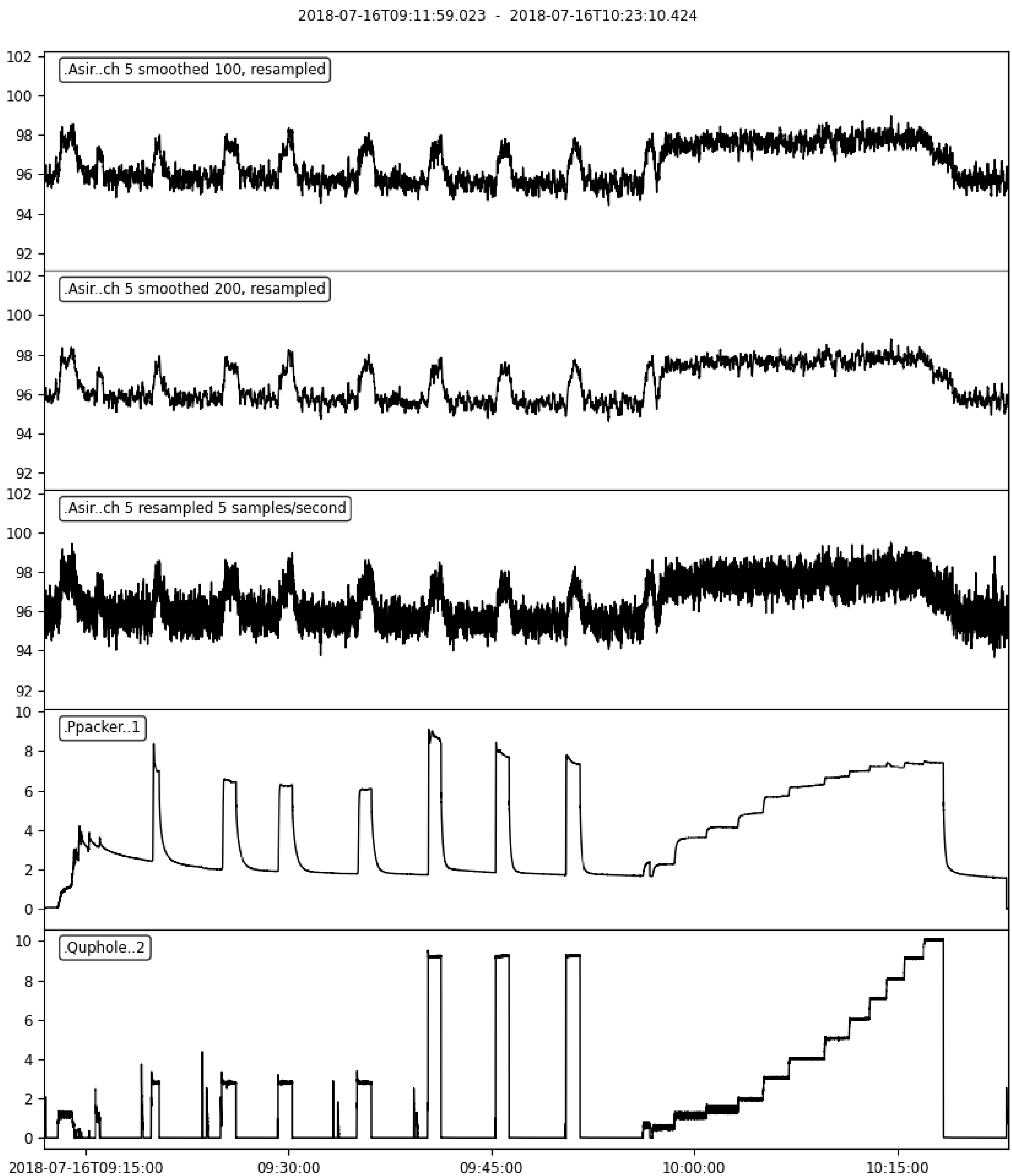

Figure S6: Broadband signal of ASIR sensor for stimulation interval HF2 51.6 m depth in the injection borehole, resampled to 5 samples per second and smoothed over 100 and 200 samples before resampling, in comparison to the recorded pressure and flow signals. Note that the pressure gauge located at the surface (Ppacker-uphole) was used for the comparison because (in contrast to Pdownhole, measuring pressure in the stimulation interval) it recorded the inflation pressure of the packers and the pressure of the

fluid entering the injection line. The flowmeter was installed in the injection line at the surface (uphole). See Figure 6 for comparison of signals recorded uphole and downhole (in the stimulation interval).

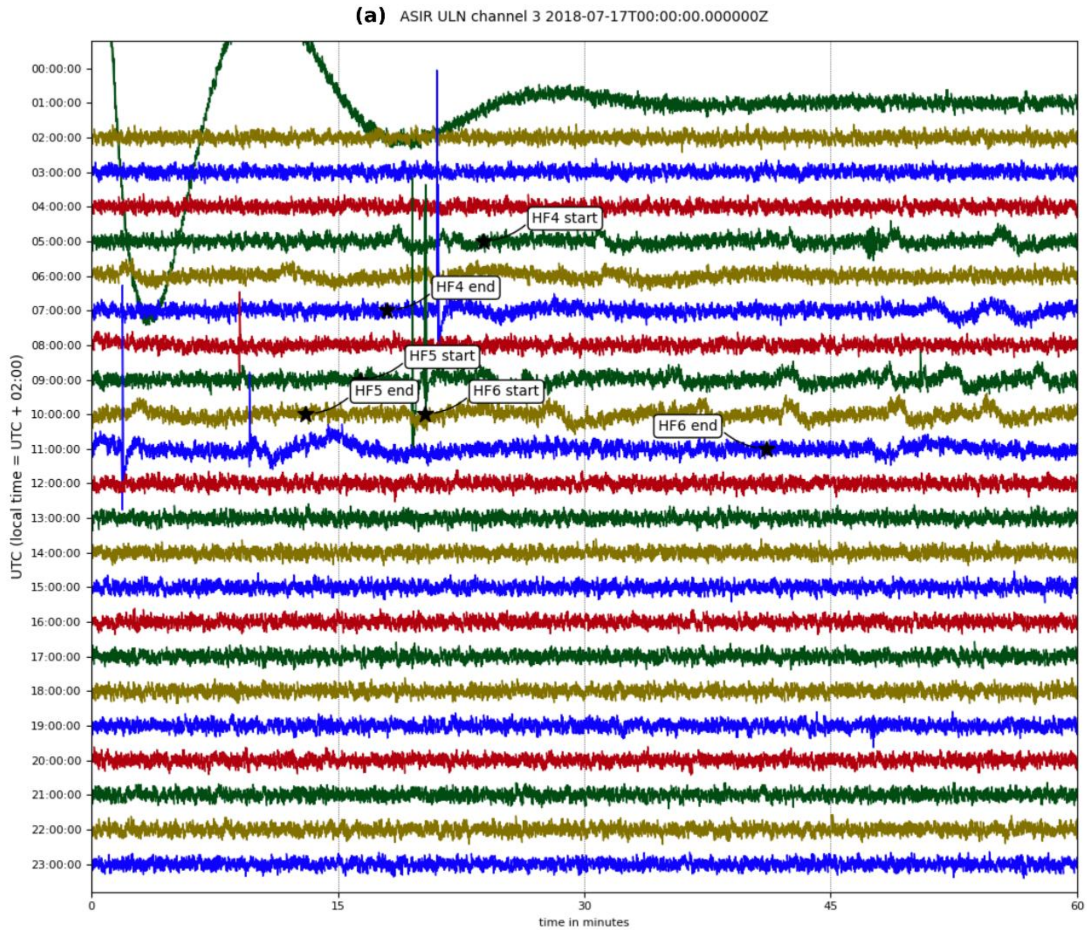

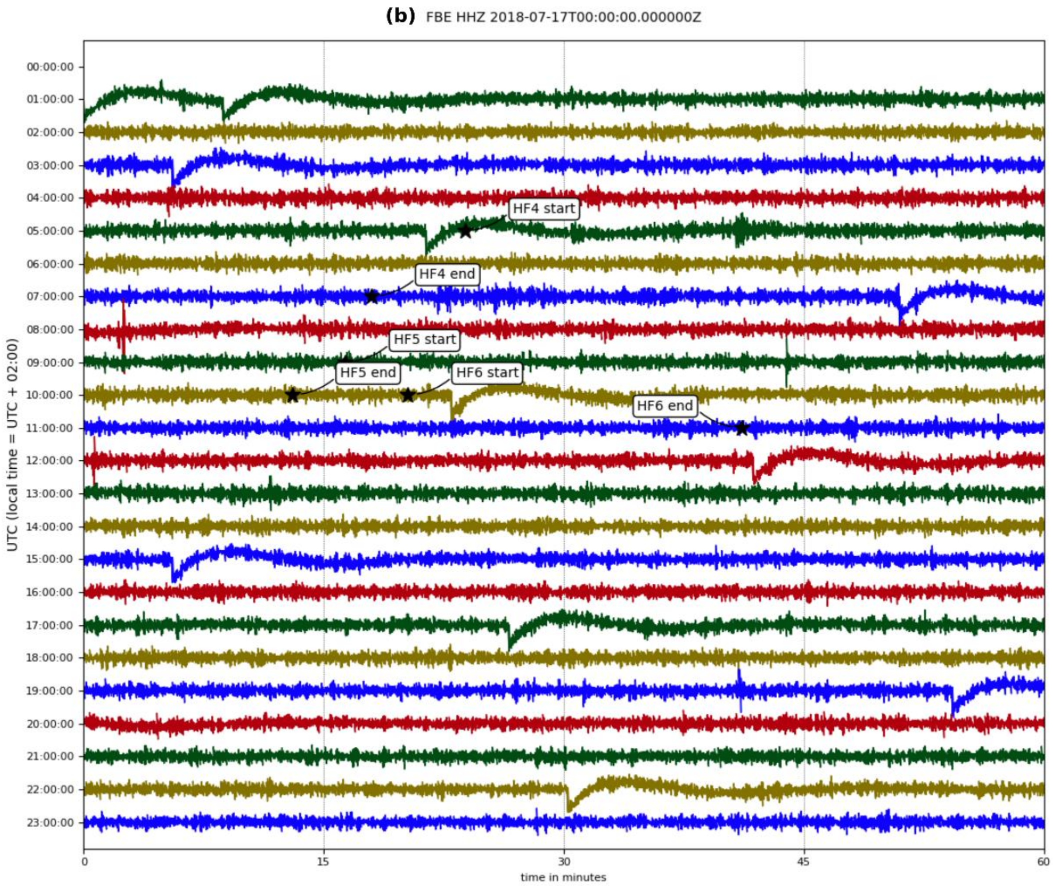
(b) FBE HHZ 2018-07-17T00:00:00.000000Z
UTC (local time = UTC + 02:00)
00:00:00
01:00:00
02:00:00
03:00:00
04:00:00
05:00:00
06:00:00
07:00:00
08:00:00
09:00:00
10:00:00
11:00:00
12:00:00
13:00:00
14:00:00
15:00:00
16:00:00
17:00:00
18:00:00
19:00:00
20:00:00
21:00:00
22:00:00
23:00:00
HF4 start
HF4 end
HF5 start
HF5 end
HF6 start
HF6 end
0
15
30
45
60
time in minutes

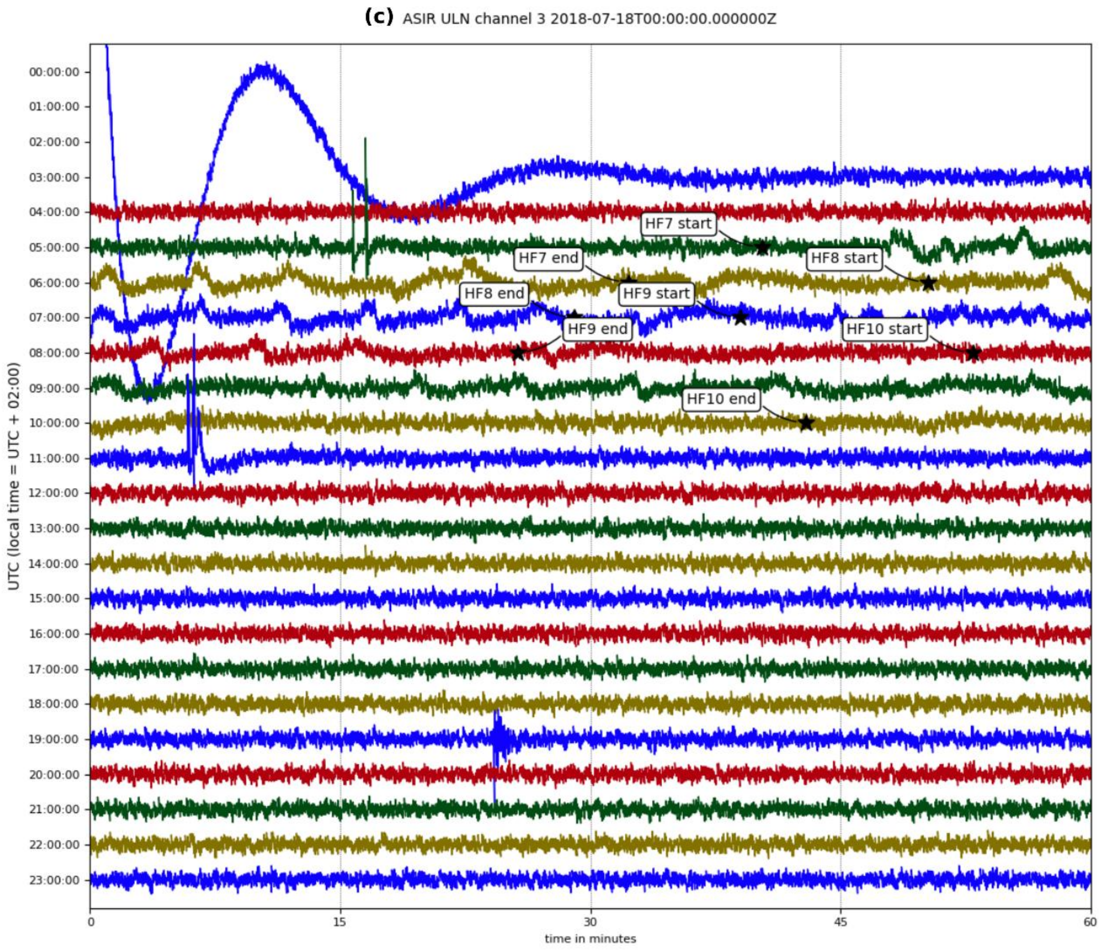
(c) ASIR ULN channel 3 2018-07-18T00:00:00.000000Z
UTC (local time = UTC + 02:00)
00:00:00
01:00:00
02:00:00
03:00:00
04:00:00
05:00:00
06:00:00
07:00:00
08:00:00
09:00:00
10:00:00
11:00:00
12:00:00
13:00:00
14:00:00
15:00:00
16:00:00
17:00:00
18:00:00
19:00:00
20:00:00
21:00:00
22:00:00
23:00:00
HF7 start
HF7 end
HF8 start
HF8 end
HF9 start
HF9 end
HF10 start
HF10 end
0
15
30
45
60
time in minutes

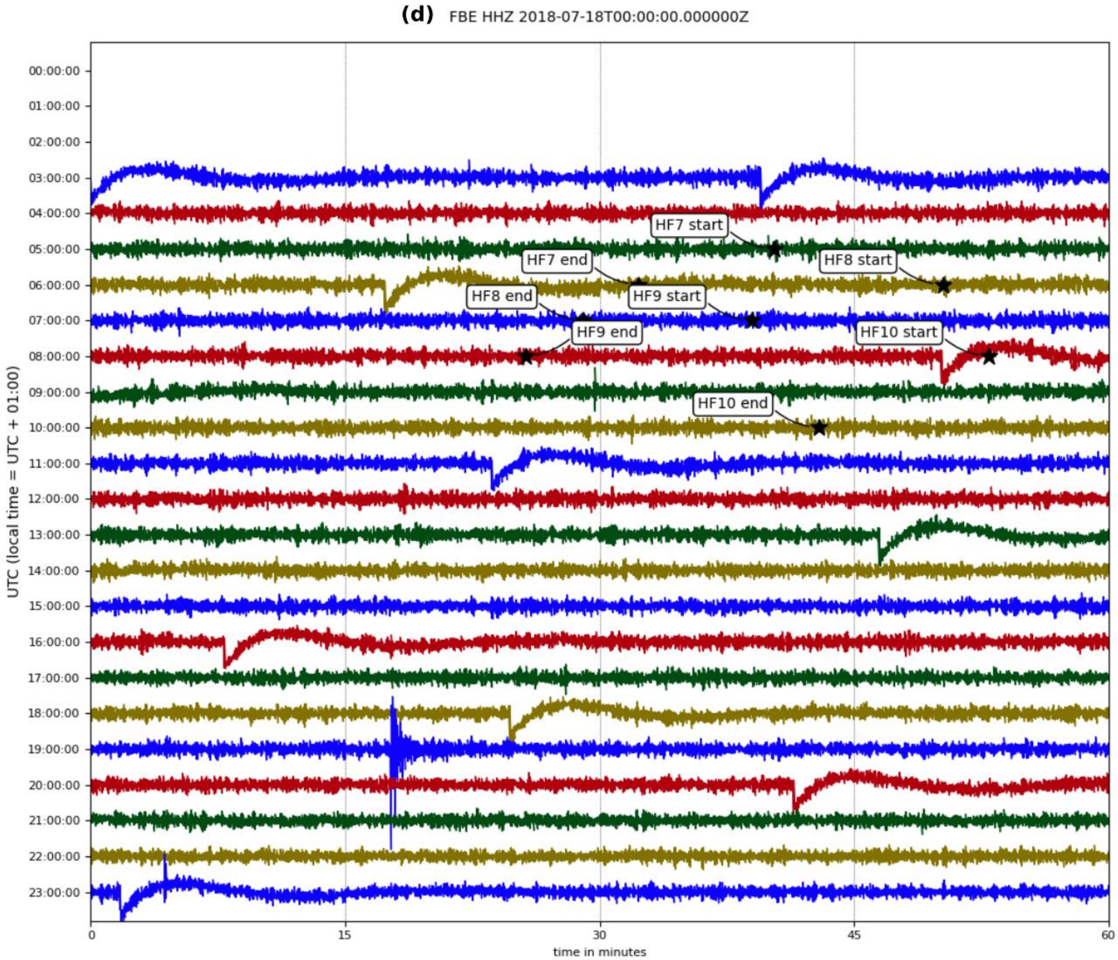

Figure S7: Daily records of the horizontal channel of the ASIR (a,c) and vertical channel FBE broadband sensor (b,d) located at Reiche Zeche mine for the second and third day of stimulation on 17 and 18 July 2018, respectively. Hydrofrac start and end times are marked (by stars and labelled) as listed in Table 2. Note that long period swings in the records result from bandpass filtering (0.001–1 Hz) in combination with data gaps as seen for the beginning of the records for the ASIR sensor and throughout the day for FBE. Some earthquakes and local quarry blasts are seen on both sensors, whereas stimulation related signals are only visible on the ASIR broadband sensor deployed at the STIMTEC site. The distance between both sensors is ca. 440 m. Note that the interpretation of some of the drops seen for the ASIR sensor remain unclear but are likely associated with sensor self-centring as determined on a shake table at GFZ lab after the experiment.

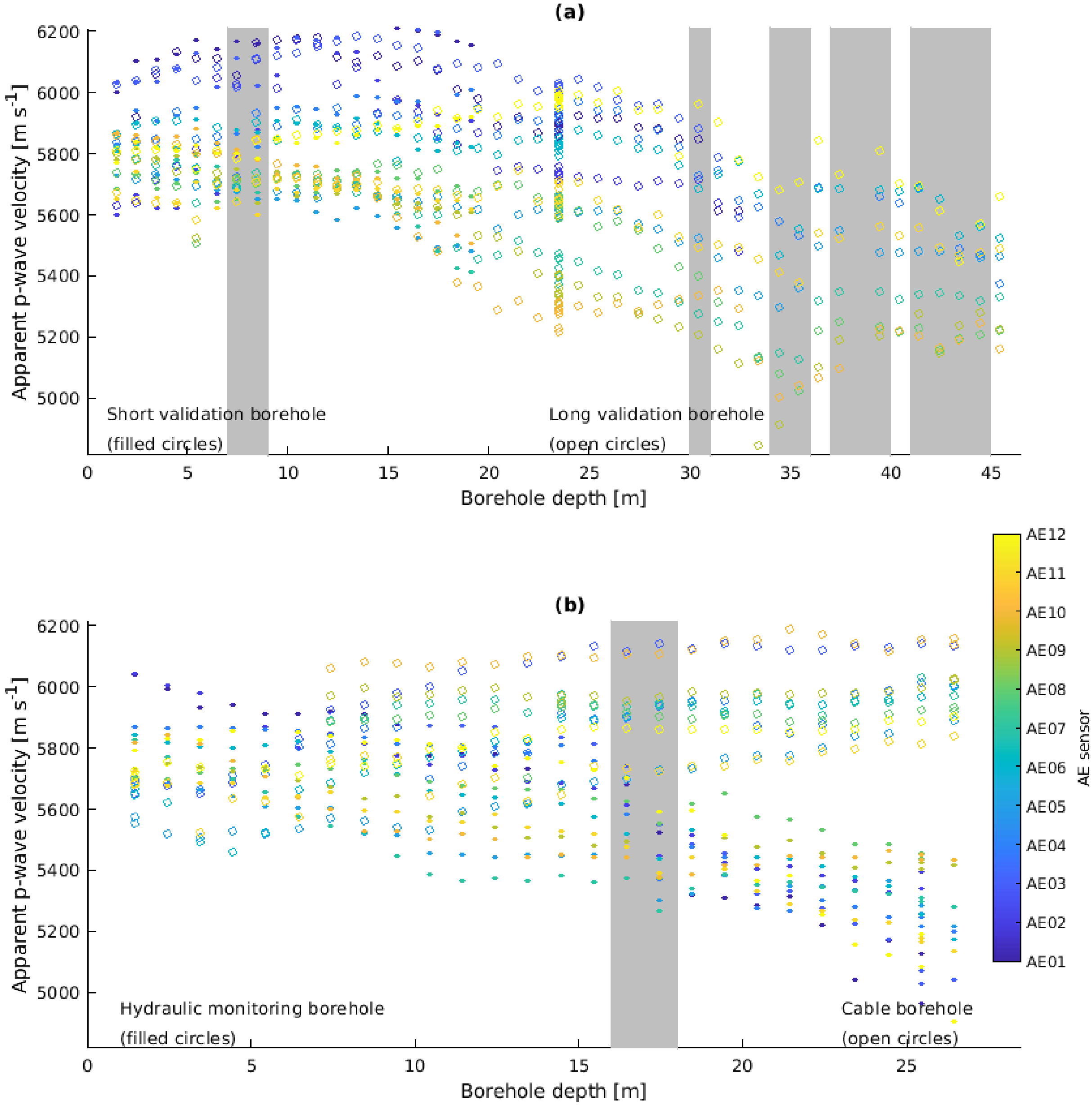
(a)
6200
6000
5800
5600
5400
5200
5000
Apparent p-wave velocity [m s-1]
Short validation borehole
(filled circles)
Long validation borehole
(open circles)
0
5
10
15
20
25
30
35
40
45
Borehole depth [m]
(b)
Hydraulic monitoring borehole
(filled circles)
Cable borehole
(open circles)
AE12
AE11
AE10
AE09
AE08
AE07
AE06
AE05
AE04
AE03
AE02
AE01
AE sensor

65

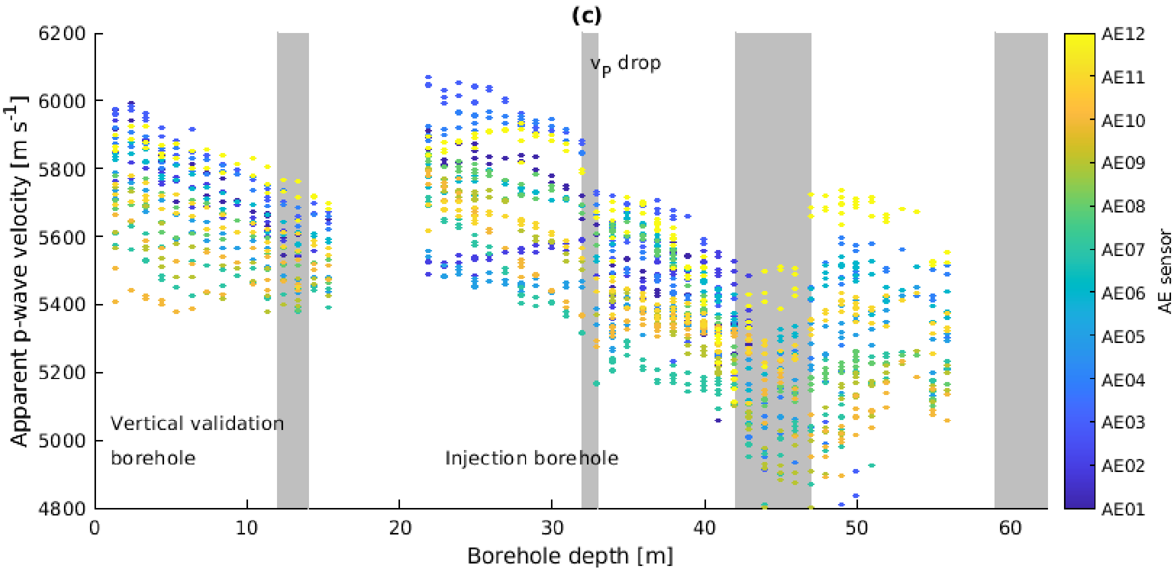

Figure S8: Apparent P-wave velocities from the UT measurements against borehole depth for different boreholes in comparison with log sections of increased fracture density and width as shown in Figure 2. a) Short and long inclined validation boreholes, b) hydraulic monitoring borehole and cable borehole, and c) vertical validation and injection boreholes.

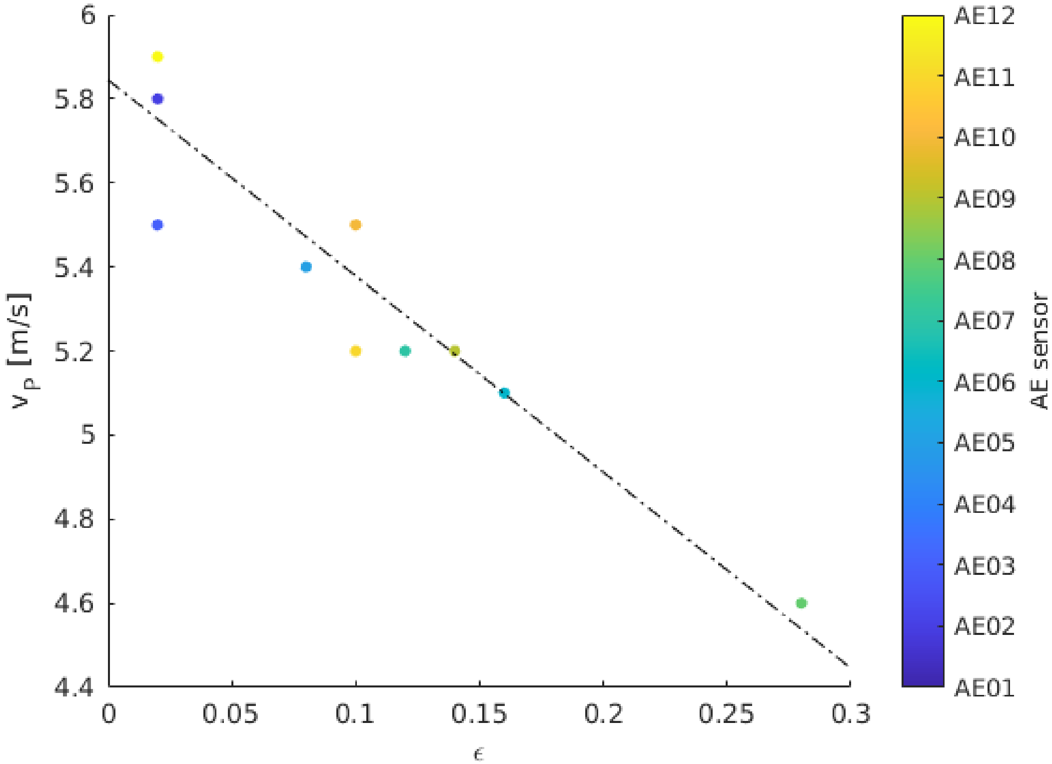

Figure S9: Trade-off in Thomsen parameters ε (strength of P-wave anisotropy) and v_{P0} (velocity along symmetry axis) for all AE sensors.